Preprints of the 19th World Congress
The International Federation of Automatic Control
Cape Town, South Africa. August 24-29, 2014

Particle Swarm Optimized Intelligent Control of Nonlinear Full-Car Electrohydraulic Suspensions

Jimoh O. Pedro * **Muhammed Dangor** *
Olurotimi A. Dahunsi * **M. Montaz Ali** **

* *School of Mechanical, Industrial and Aeronautical Engineering, University of the Witwatersrand, 1 Jan Smuts Avenue, Private Bag 03, WITS 2050, Johannesburg, South Africa (e-mail: jimoh.pedro@wits.ac.za, mdangor98@gmail.com,tundedahunsi@gmail.com).*
** *School of Computational and Applied Mathematics, Faculty of Science, and TCSE, Faculty of Engineering and Built Environment, University of the Witwatersrand, 1 Jan Smuts Avenue, Private Bag 03, WITS 2050, Johannesburg, South Africa (e-mail: montaz.ali@wits.ac.za)*

Abstract: This paper presents the design of an indirect adaptive feedback linearization (FBL)-based control using dynamic neural networks (DNN) for full-car nonlinear electrohydraulic suspensions. Particle swarm optimization (PSO) algorithm is used in training the DNN to learn the dynamics of the system. A multi-loop, PSO-optimized proportional-integral-derivative (PID) control is implemented for the feedback-linearized DNN model to improve system performance. The proposed control scheme outperformed the passive vehicle suspension system (PVSS) and the benchmark PSO-optimized PID controller.

Keywords: Active vehicle suspension, Feedback linearization, Dynamic neural networks, Particle swarm optimization, PID control, Force feedback

1. INTRODUCTION

Resolving the conflicting nature of performance requirements such as ride comfort, handling and road holding has been a major concern for the design of active vehicle suspension systems (AVSS) Pedro et al. (2013). AVSS have significantly resolved this conflict, but the tuning of controller gains is still a limiting factor in the design process.

Linear control methods such as PID, $\mathcal{H}_2$, $\mathcal{H}_\infty$, linear quadratic regulator (LQR), and linear quadratic Gaussian (LQG) have been incorporated on AVSS. Their application for realistic nonlinear systems requires a great deal of intuitive reasoning, experience and rigorous fine tuning. Heuristic optimization principles such as controlled random search (CRS), genetic algorithm (GA), differential evolution (DE), pattern search (PS) and PSO have been used to select controller gains for AVSS Pedro et al. (2013). Vast majority of these have only addressed linear systems without actuator dynamics Wai et al. (2011); Crews et al. (2011); Chiou et al. (2012).

A realistic study must incorporate the vehicle lateral and longitudinal dynamics in order to create a successful control method. Pedro et al. (2013) applied DE algorithm to resolve the conflicting performance criteria for full-car PID-controlled AVSS. Drawbacks of such controllers involve the generation of high controller gains, chattering, and poor robustness to parameter variations and uncertainties.

Nonlinear and intelligent adaptive control schemes such as FBL, sliding mode control (SMC) and backstepping have been developed to address these drawbacks. SMC has been successfully applied for nonlinear half-car AVSS that contain a considerable degree of coupling Yagiz et al. (2008). Neural control and fuzzy logic control (FLC) have been applied for a variety of nonlinear quarter-car, half-car and full-car AVSS with actuator dynamics Eski and Yildirim (2009); Aldair and Wang (2010); Guclu and Gulez (2008); Lin et al. (2009); Pekgokgoz et al. (2010); Chiou et al. (2012). Improved performance and robustness were observed through their use. Hybrid approaches with both linear and nonlinear control laws have also been developed. An indirect adaptive control was also performed for a quarter-car AVSS using a multilayer perceptron (MLP) neural network (NN) Pedro and Dahunsi (2011). Pekgokgoz et al. (2010); Chiou et al. (2012) employed GA and PSO-based tuning methods for adaptive fuzzy PID-controllers to improve system performance. Alfi and Fateh (2011) applied PSO to train a NN for system identification.

DNN have not been extensively applied for intelligent control of AVSS because the static neural networks have been reliable up until now. DNN contain recurrent elements

which are modelled using differential equations. Garces et al. (2003) presented a practical approach to DNN-based FBL control for a class of nonlinear SISO and MIMO systems.

This paper presents a realistic DNN-based hybrid FBL control for nonlinear electrohydraulic full-car AVSS using PSO algorithm to optimize the networks weights and controller gains tuning. The paper is organized as follows: the system model is presented in section 2. Section 3 introduces the AVSS performance specifications followed by a brief description of the PID controller. PSO algorithm is also described in this section. Detailed description of the DNN-based system identification and FBL control are presented. Section 4 presents simulation results with discussion and the paper is concluded in section 5.

2. SYSTEM OVERVIEW AND MODELLING

Figure 1 shows the schematic of the full-car system used in this paper. Four suspension systems placed at each wheel support the vehicle body Pedro et al. (2013).

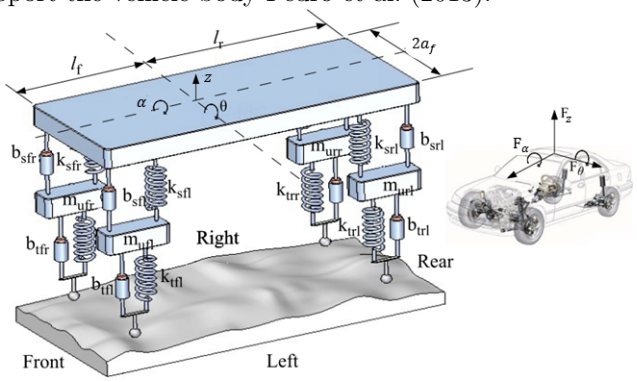

Fig. 1. Schematic of the full-car model

Applications of Newton's second law of motion to the nonlinear full-car AVSS gives the governing equations in state-space form as Pedro et al. (2013); Noura et al. (2009):

$$\dot{\mathbf{x}} = \mathbf{f}(\mathbf{x}) + \mathbf{g_1}(\mathbf{x})u_1 + \mathbf{g_2}(\mathbf{x})u_2 + \mathbf{g_3}(\mathbf{x})u_3 + \mathbf{g_4}(\mathbf{x})u_4 + \mathbf{w}(\mathbf{x}), \quad (1)$$

with the state vector defined as:

$$\begin{aligned}\mathbf{x} &= [x_1, x_2, \ldots, x_{22}]^T \\ &= [z_{tfr}, \dot{z}_{tfr}, P_{Lfr}, x_{vfr}, z_{tfl}, \dot{z}_{tfl}, P_{Lfl}, x_{vfl}, z_{trr}, \dot{z}_{trr}, \\ &\quad P_{Lrr}, x_{vr}, z_{trl}, \dot{z}_{trl}, P_{Lrl}, x_{vrl}, z, \dot{z}, \theta, \dot{\theta}, \alpha, \dot{\alpha}\Big]^T, \end{aligned} \quad (2)$$

where z_{tfr}, z_{trr}, z_{tfl} and z_{trl} are the front right, rear right, front left and rear left wheel displacements respectively; $\dot{z}_{tfr}$, $\dot{z}_{trr}$, $\dot{z}_{tfl}$, and $\dot{z}_{trl}$ are the front right, rear right, front left and rear left wheel vertical velocities respectively; P_{Lfr}, P_{Lrr}, P_{Lfl}, and P_{Lrl} are the pressure drops across the front right, rear right, front left and rear left differences experienced across the hydraulic pistons respectively; x_{vfr}, x_{vrr}, x_{vfl}, and x_{vrl} are the front right, rear right, front left and rear left spool-valve displacements respectively; z and $\dot{z}$ are the body vertical displacement and velocity respectively; θ and $\dot{\theta}$ are the body pitch angular displacement and velocity respectively; and α and $\dot{\alpha}$ are the body roll angular displacement and velocity respectively. The system outputs are defined as:

$$y_{fr} = h_{fr}(\mathbf{x}) = x_1 - (x_{17} - l_f \sin x_{19} + (a_f/2)\sin x_{21}), \quad (3)$$
$$y_{fl} = h_{fl}(\mathbf{x}) = x_5 - (x_{17} - l_f \sin x_{19} - (a_f/2)\sin x_{21}), \quad (4)$$
$$y_{rr} = h_{rr}(\mathbf{x}) = x_9 - (x_{17} + l_f \sin x_{19} + (a_f/2)\sin x_{21}), \quad (5)$$
$$y_{rl} = h_{rl}(\mathbf{x}) = x_{13} - (x_{17} + l_f \sin x_{19} - (a_f/2)\sin x_{21}). \quad (6)$$

System matrices $\mathbf{f}$ and $\mathbf{g}$ and disturbance input matrix $\mathbf{w}$ are:

$$\mathbf{f}(\mathbf{x}) = [\, f_1(\mathbf{x})\ f_2(\mathbf{x})\ \ldots\ \ldots\ \ldots\ f_{22}(\mathbf{x})\,]^T, \quad (7)$$
$$\mathbf{g_1}(\mathbf{x}) = [\,0\ \ldots\ g_4(\mathbf{x})\ \ldots\ \ldots\ \ldots\ 0\,]^T, \quad (8)$$
$$\mathbf{g_2}(\mathbf{x}) = [\,0\ \ldots\ \ldots\ g_8(\mathbf{x})\ \ldots\ \ldots\ 0\,]^T, \quad (9)$$
$$\mathbf{g_3}(\mathbf{x}) = [\,0\ \ldots\ \ldots\ \ldots\ g_{12}(\mathbf{x})\ \ldots\ 0\,]^T, \quad (10)$$
$$\mathbf{g_4}(\mathbf{x}) = [\,0\ \ldots\ \ldots\ \ldots\ \ldots\ g_{16}(\mathbf{x})\ 0\,]^T, \quad (11)$$
$$\mathbf{w}(\mathbf{x}) = [\,0\ w_2(\mathbf{x})\ \ \ldots\ w_{10}(\mathbf{x})\ \ldots\ w_{14}(\mathbf{x})\ \ldots\,]^T. \quad (12)$$

The elements of the input matrices $\mathbf{g_1}(\mathbf{x})$, $\mathbf{g_2}(\mathbf{x})$, $\mathbf{g_3}(\mathbf{x})$ and $\mathbf{g_4}(\mathbf{x})$ are of the form:

$$g_4(\mathbf{x}) = K_{vfr}/\tau_{fr}, \quad g_8(\mathbf{x}) = K_{vfl}/\tau_{fl}, \quad (13)$$
$$g_{12}(\mathbf{x}) = K_{vrr}/\tau_{rr}, \quad \text{and} \quad g_{16}(\mathbf{x}) = K_{vrl}/\tau_{rl}. \quad (14)$$

Disturbance matrix $\mathbf{w}(\mathbf{x})$ terms are:

$$w_2(\mathbf{x}) = (k_{tfr}w_{fr} + b_{tfr}\dot{w}_{fr})/m_{ufr}, \quad (15)$$
$$w_6(\mathbf{x})) = (k_{tfl}w_{fl} + b_{tfr}\dot{w}_{fl})/m_{ufl}, \quad (16)$$
$$w_{10}(\mathbf{x}) = (k_{trr}w_{rr} + b_{trr}\dot{w}_{rr})/m_{urr}, \quad (17)$$
$$w_{14}(\mathbf{x}) = (k_{trl}w_{rl} + b_{trl}\dot{w}_{rl})/m_{url}. \quad (18)$$

This form is required to examine if the system is input-output feedback linearizable. The effectiveness of the proposed controller is tested by exposing the vehicle to a deterministic road bump with varying height. The road profile at each wheel and the values of the system parameters used in this study are the same as given in Pedro et al. (2013).

3. CONTROLLER IMPLEMENTATION

The chosen specifications are based on constraints of the physical model and are also aimed at improving ride comfort, road holding and vehicle handling from that of the PVSS. The performance index is Pedro et al. (2013):

$$\begin{aligned} J &= J_1 + J_2 + J_3 + J_4 + J_5 \\ &= \frac{1}{T}\int_0^T \left[\left(\frac{\ddot{z}}{\ddot{z}_{max}}\right)^2 + \left(\frac{\ddot{\theta}}{\ddot{\theta}_{max}}\right)^2 + \left(\frac{\ddot{\alpha}}{\ddot{\alpha}_{max}}\right)^2\right] dt + \\ &\quad \sum_{j=fr}\sum_{i=rl}\frac{1}{T}\int_0^T \left[\left(\frac{F_{kt_{ij}} + F_{bt_{ij}}}{(F_{kt_{ij}} + F_{bt_{ij}})_{max}}\right)^2\right] dt + \\ &\quad \sum_{i=1}^{4}\frac{1}{T}\int_0^T \left[\left(\frac{y_i}{y_{i_{max}}}\right)^2 + \left(\frac{u_i}{u_{i_{max}}}\right)^2\right] dt + \\ &\quad \sum_{j=fr}\sum_{i=rl}\frac{1}{T}\int_0^T \left(\frac{F_{a_{ij}}}{F_{a_{ij_{max}}}}\right)^2 dt, \end{aligned} \quad (19)$$

where J_1 addresses ride comfort and vehicle handling with the maximum permitted heave acceleration $\ddot{z}_{max}$, pitch acceleration $\ddot{\theta}_{max}$, and roll acceleration $\ddot{\alpha}_{max}$. J_2, J_3, J_4 and J_5 pertain to tyre dynamic load, suspension travel, control input voltage and actuation force respectively with $(F_{ktij} + F_{btij})_{max}$, $y_{ij_{max}}$, $F_{a_{ij_{max}}}$ and $u_{ij_{max}}$ signifying the maximum allowable limits in each of these aspects.

3.1 PID Controller Design

PID control is the most widely used controller for AVSS applications. It serves as a good benchmark of comparison for the proposed intelligent controller. The PID controller architecture proposed in this study is the same as in Pedro et al. (2013). Controller gains are selected with Ziegler-Nichols method, after which fine tuning is conducted with the objective of minimizing the performance index J. The performance index achieved through this process is 3.2, which is substantially superior to that of the PVSS.

3.2 Particle Swarm Optimization Algorithm

We create an F-dimensional space, where F is the number of problem variables being optimized. These correspond to the DNN parameters for system identification and the controller gains in controller optimization. Each problem variable represents a specific dimension. A set of problem variables called a "particle" is placed within this F-dimensional space, where its position in each dimension corresponds to the magnitude of its problem variable in its associating dimension. Firstly, random sets of particles are generated in a bounded space chosen through intuitive knowledge. The performance of the particle is defined according to its performance index J. In each iteration each particle is set to move at a random degree to the best particle in the space $\mathbf{G}_{best}$ as well as to their best individually recorded best position $\mathbf{P}_{best}$. This algorithm may be summarized as follows Alfi and Fateh (2011); Kennedy and Eberhart (1999); Chiou et al. (2012):

1 Generate a population set of particles $(\mathbf{x_0}, \mathbf{x_1}, .., \mathbf{x_N})$.
2 Compute global best particle in the population.
3 Check stopping criterion, proceed to step 7 if stopping criterion is met, otherwise continue to next step.
4 Compute the positions of each particle $\mathbf{x}(t+1)$ with the relations

$$\mathbf{x}(t+1) = \mathbf{x}(t) + \mathbf{V}(t+1) \tag{20}$$

where $\mathbf{x}$ holding the position of each particle, $t+1$ refers to the next iteration, $\mathbf{V}$ is the velocity matrix which computes the degree to which each particle moves in the search space. It is determined as follows:

$$\begin{aligned}\mathbf{V}(t+1) = w_1\mathbf{V}(t) + w_2 rand1(1,F)(\mathbf{P}_{best} - \mathbf{x}(t)) \\ + w_3 rand2(1,F)(\mathbf{G}_{best} - \mathbf{x}(t))\end{aligned} \tag{21}$$

where $\mathbf{G}_{best}$ is the set of problem variables that produced the best results thus far, $\mathbf{P}_{best}$ is a matrix constraining the individual best positions of each particle, $(\mathbf{P}_{best} - \mathbf{x}(t))$ is called the local search vector and $(\mathbf{G}_{best} - \mathbf{x}(t))$ is the global search vector, w_1 is the inertia weight, w_2 and w_3 are the learning rates, $rand1(1,F)$ and $rand2(1,F)$ are uniformly distributed random numbers between 0 and 1.

5 Update personal best and global best particles using Chiou et al. (2012):

$$\mathbf{A}(t+1) = \begin{cases} x_i(t+1) & \text{if } f(x_i(t+1)) < f(\mathbf{A}(t)) \\ \mathbf{A}(t) & \text{if } f(x_i(t+1)) \geq f(\mathbf{A}(t)) \end{cases} \tag{22}$$

$$\mathbf{B}(t+1) = \arg\min_{\mathbf{A}} f(\mathbf{A}(t+1)), \tag{23}$$

where $f(\ldots)$ denotes the respective performance index J of the various particles, $\mathbf{A}$ and $\mathbf{B}$ represent $\mathbf{P}_{best_i}$ and $\mathbf{G}_{best_i}$ respectively.
6 Return to step 3.
7 The optimal solution is chosen to be the global best particle.

3.3 DNN-Based Feedback Linearization Control

Figure 2 shows the architecture of the proposed control scheme (DNNFBL+PSO). It is an indirect adaptive controller where the system dynamics are learnt using DNN which are trained offline with PSO algorithm. FBL is later applied to the DNN models to create a linear decoupled relationship between υ_{ij} and y_{ij}. The controller gains are computed with a separate PSO algorithm which minimizes the performance index, Eq. (19).

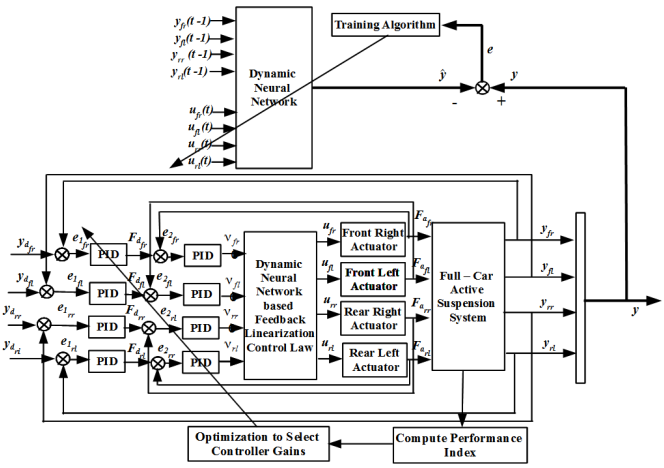

Fig. 2. Schematic of the proposed full-car indirect adaptive intelligent controller

3.4 NN-Based Nonlinear System Identification

The system identification involves using four independent DNN models to learn the plant dynamics at each wheel for the operating frequency range $(0.5Hz,\ 80Hz)$ European Commission (2002); Dahunsi et al. (2010). A white band limited (WBL) noise covering this range is chosen as the input data for the system identification process. These WBL noise inputs are constrained to $\pm 10V$. The output data arising from these inputs is also constrained to ± 0.1m. Additionally, the input data at the various suspension systems must be significantly different in order to account for the coupling within the system. The properties of the WBL input data at each wheel are as follows: u_{fr}: seed strength of 23341, noise power of 0.1; u_{rr}: seed strength of 22641, noise power of 0.07; u_{fl}: seed strength of 22641, noise power of 0.08; and u_{rl}: seed strength of 22641, noise power of 0.05. A uniform sampling time of $0.001s$ is used for the input at each wheel.

Each of the DNN models is described as follows:

$$\begin{aligned}\dot{x}_{ij} = &-\beta_{ij}\mathbf{x} + \mathbf{W}_{ij}\sigma(\mathbf{x_{ij}}) + \mathbf{g}_{1_{ij}}(\mathbf{x})u_{fr} + \mathbf{g}_{2_{ij}}(\mathbf{x})u_{fl} \\ &+\mathbf{g}_{3_{ij}}(\mathbf{x})u_{rr} + \mathbf{g}_{4_{ij}}(\mathbf{x})u_{rl} + \gamma_{1_{ij}}(\mathbf{x})y_{fr}(t-1) \\ &+\gamma_{2_{ij}}(\mathbf{x})y_{fl}(t-1) + \gamma_{3_{ij}}(\mathbf{x})y_{rr}(t-1) \\ &+\gamma_{4_{ij}}(\mathbf{x})y_{rl}(t-1), \end{aligned} \tag{24}$$

$$\hat{y}_{ij} = \hat{h}_{ij}(\mathbf{x}) = \sum_{L=1}^{n_n} \mathbf{w_{ij_L}}\mathbf{x_{ij_1}}, \tag{25}$$

with $\mathbf{x}_{ij}$ denoting outputs from each neuron, β is the matrix of time constants of each neuron, $\sigma(\mathbf{x})$ is the activation function, which is the hyperbolic tangent function specifically chosen to ensure stability Garces et al. (2003), $\mathbf{W}_{ij}$ is the interconnecting weighting matrix of outputs, u_{ij} is the previous control inputs, $\mathbf{g}_{k_{ij}}$ is the weighting matrix of inputs, $y_{ij}(t-1)$ is the delayed actual system outputs fed into the DNN, and $\gamma_{\mathbf{k_{ij}}}$ are their respective weightings. $\mathbf{w}_{ij}$ is the weightings for the second layer, n_n is the number of neurons in the hidden layer. The following may be defined to simplify the FBL law to be applied to the DNN later:

$$\begin{aligned}\dot{\mathbf{x}}_{\mathbf{ij}} = &\mathbf{f_{ij}} + \mathbf{g}_{1_{ij}}(\mathbf{x})u_{fr} + \mathbf{g}_{2_{ij}}(\mathbf{x})u_{fl} + \mathbf{g}_{3_{ij}}(\mathbf{x})u_{rr} \\ &+\mathbf{g}_{4_{ij}}(\mathbf{x})u_{rl}\gamma_{1_{ij}}(\mathbf{x})y_{fr}(t-1) + \gamma_{2_{ij}}(\mathbf{x})y_{fl}(t-1) \\ &+\gamma_{3_{ij}}(\mathbf{x})y_{rr}(t-1) + \gamma_{4_{ij}}(\mathbf{x})y_{rl}(t-1), \end{aligned} \tag{26}$$

where:

$$\mathbf{f_{ij}} = -\beta_{\mathbf{ij}}\mathbf{x_{ij}} + \mathbf{W}_{ij}\sigma(\mathbf{x}). \tag{27}$$

The properties of each DNN is chosen using pruning method Norgaard et al. (2000). Basically, the DNN configuration is altered until satisfactory topology and structure similar to the actual system output is attained for the DNN predicted output $\hat{y}_{ij}$. Numerical experiments for various number of hidden layer neurons reveal that 13 neurons give satisfactory results.

The performance index of each DNN is the mean squared error (MSE) between the predicted and the actual system outputs:

$$J_{ij} = MSE = \frac{1}{2M}\sum_{i=0}^{M}(y_{ij} - \hat{y}_{ij})^2, \tag{28}$$

where M is the number of samples in the input-output data set. The DNN is trained using PSO algorithm. The settings of the PSO algorithm used for the selection of the networks weightings are: population size, $N = 100$; maximum number of iterations, $k_{max} = 50$; and optimization parameters, $w_1 = 0.5$, $w_2 = w_3 = 2$. The convergence history of the MSE for each suspension system is shown in Figure 3. The training and validation results for the rear right suspension system are presented in Figures 4 and 5 respectively.

3.5 AVSS DNN-Based Input-Output Feedback Linearization

The FBL law will be applied to the DNN models. The system outputs are defined as follows:

$$\hat{y}_{fr} = \hat{h}_{fr}(\mathbf{x}),\ \hat{y}_{fl} = \hat{h}_{fl}(\mathbf{x}),\ \hat{y}_{rr} = \hat{h}_{rr}(\mathbf{x}),\ \hat{y}_{rl} = \hat{h}_{rl}(\mathbf{x}) \tag{29}$$

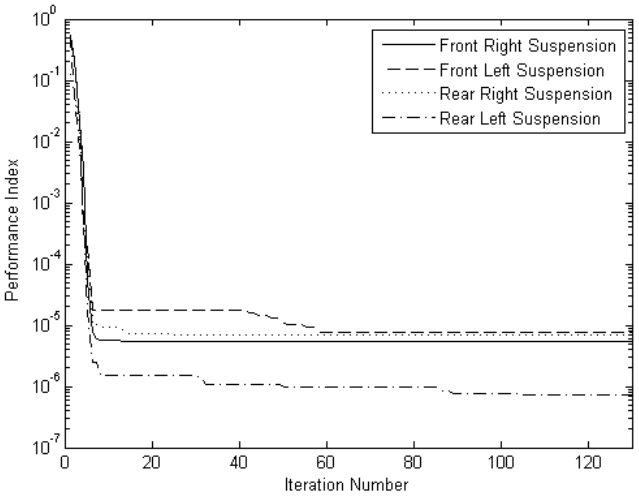

Fig. 3. Convergence of MSE through PSO-based DNN learning

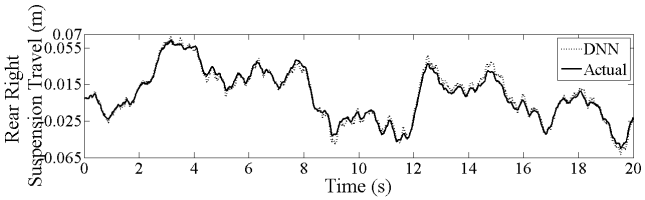

Fig. 4. DNN identification tracking of rear right suspension system

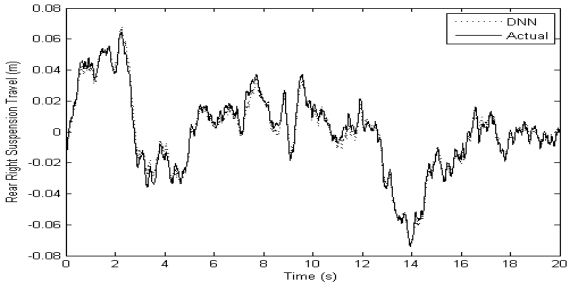

Fig. 5. DNN validation tracking of rear right suspension system

The first time derivatives of each of these outputs are:

$$\begin{aligned}\dot{\hat{y}}_{ij} &= \frac{\partial \hat{y}_{ij}}{\partial t} = \frac{\partial \hat{y}_{ij}}{\partial \mathbf{x}_{ij}}\frac{\partial \mathbf{x}_{ij}}{\partial t} = \frac{\partial \hat{h}_{ij}(\mathbf{x})}{\partial \mathbf{x}}\dot{\mathbf{x}}_{ij} \\ &= w_{ij_1}\left[-\beta_{ij_1}x_1 + \sum_{k=1}^{13} W_{ij_{1k}}\sigma(x_k)\right] = \mathcal{L}_{f_{ij}}\hat{h}_{ij}(\mathbf{x}). \end{aligned} \tag{30}$$

Each of which is not explicitly a function of the system inputs. It can shown that the second time derivative depends on the system inputs.

$$\begin{aligned}\ddot{\hat{y}}_{ij} &= \frac{\partial^2 \hat{y}_{ij}}{\partial t^2} = \frac{\partial \frac{\partial \hat{y}_{ij}}{\partial t}}{\partial \mathbf{x}_{ij}}\frac{\partial \mathbf{x}_{ij}}{\partial t} = \frac{\partial \mathcal{L}_f \hat{h}_{ij}(\mathbf{x}_{ij})}{\partial x}\dot{\mathbf{x}}_{ij} \\ &= d_{ij}(\mathbf{x}) + e_{ij}(\mathbf{x})u_{ij} = \mathcal{L}^2_{f_{ij}}\hat{h}_{ij}(\mathbf{x}) + \mathcal{L}_{g_{ij}}\mathcal{L}_{f_{ij}}\hat{h}_{ij}(\mathbf{x})u_{ij}, \end{aligned} \tag{31}$$

with nonlinear functions $d_{ij}(\mathbf{x})$ and $e_{ij}(\mathbf{x})$ of which signify the free and forced response of the system respectively. The vector of relative degree $\mathbf{r}$ has the form:

$$\mathbf{r} = [\, r_{fr}\ r_{fl}\ r_{rr}\ r_{rl}\,]^T = [\,2\ 2\ 2\ 2\,]^T. \tag{32}$$

Since the relative degree is less than the number of states (i.e. 13), the DNN models are input-output feedback linearizable. The system dynamics may be expressed in terms of the characteristic matrix $\hat{\mathbf{A}}(\mathbf{x})$ Garces et al. (2003):

$$\ddot{\mathbf{y}} = f(\mathbf{x}, \mathbf{u}) = \hat{\mathbf{A}}(\mathbf{x}) + \hat{\mathbf{B}}(\mathbf{x})\mathbf{u}. \tag{33}$$

A new transformed system is described as:

$$\hat{z} = \hat{\Psi}(\mathbf{x}) = \left[\, \hat{\xi} \;\; \hat{\eta} \,\right]^T, \tag{34}$$

with observable dynamics $\hat{\xi}_{ij} = [\, \hat{z}_{ij_1} \;\; \hat{z}_{ij_2} \,]^T$, and zero dynamics $\hat{\eta}_{ij} = \left[\, \hat{\psi}_{ij_1}(\mathbf{x}) \;\; \hat{\psi}_{ij_2}(\mathbf{x}) \;\; \ldots \;\; \hat{\psi}_{ij_{11}}(\mathbf{x}) \,\right]^T$. The new coordinate system is of the form:

$$\dot{\hat{\xi}}_{ij} = \hat{\mathbf{A}}_{c_{ij}} \hat{\xi}_{ij} + \hat{\mathbf{B}}_{c_{ij}} \hat{v}_i + \hat{\bar{\mathbf{p}}}_{ij}(w), \tag{35}$$

$$\hat{y}_{ij} = \hat{\mathbf{C}}_{c_{ij}} \xi_{ij}. \tag{36}$$

For the linear decoupled system between the virtual control input υ_{ij} and system outputs y_{ij}, the system matrices take the ensuing form:

$$\hat{\mathbf{A}}_c = \begin{bmatrix} 0 & 1 \\ \lambda_{0_{r_{ij}}} & \lambda_{1_{r_{ij}}} \end{bmatrix}, \quad \hat{\mathbf{B}}_c = \begin{bmatrix} 0 \\ 1 \end{bmatrix}, \tag{37}$$

$$\hat{\mathbf{C}}_c = [\, 1 \;\; 0 \,]^T, \quad \hat{\bar{\mathbf{p}}}(w) = [\, 0 \;\; 1 \,]^T, \tag{38}$$

υ is determined by applying inversion to Eq. (33).

$$\mathbf{u} = \hat{\mathbf{P}}(\mathbf{x}) + \hat{\mathbf{Q}}(\mathbf{x})\upsilon, \tag{39}$$

where, $\hat{\mathbf{P}}(\mathbf{x}) = -\hat{\mathbf{A}}(\mathbf{x})^{-1}\hat{\mathbf{B}}(\mathbf{x})$, and $\hat{\mathbf{Q}}(\mathbf{x}) = -\hat{\mathbf{A}}(\mathbf{x})^{-1}$. Design parameters $\lambda_{0_{r_{ij}}}$, $\lambda_{1_{r_{ij}}}$, $\lambda_{2_{r_{ij}}}$, may be added to augment performance Garces et al. (2003).

The new linear and decoupled system now becomes:

$$\sum_{k=0}^{r_{ij}} \lambda + k_{r_{ij}} \frac{d^k \hat{y}_{ij}}{dt^k} = \hat{v}_{ij}, \tag{40}$$

where the closed-loop transfer function is:

$$\hat{G}_{ij}(s) = \frac{\hat{Y}_{ij}(s)}{\hat{V}_i(s)} = \frac{1}{\lambda_{2_{r_{ij}}} s^2 + \lambda_{1_{r_{ij}}} s + \lambda_{0_{r_{ij}}}}. \tag{41}$$

Routh-Hurwitz stability criterion is applied to the denominator of the transfer function. This demands that all poles lie in the negative half plane. The new virtual control $\bar{v}_{ij}$ can be supplanted to this linear system as follows:

$$\hat{v}_{ij} = -\sum_{k=0}^{r_{ij}} \lambda_{k_{r_{ij}}} \frac{d^k \hat{y}_{ij}}{dt^k} \bar{v}_{ij}. \tag{42}$$

The controller gains of the DNNFBL and PID controller are selected using PSO as it is an efficient and quicker alternative to fine tuning. The problem variables are the controller gains and the objective function is given by Eq. (19). The following settings of the PSO algorithm are used: population size, $N = 100$; maximum number of iteration, $k_{max} = 150$; and optimization parameters, $w_1 = 0.5$, $w_2 = w_3 = 2$ and the performance index convergence is shown in Figure 6.

The PSO-based DNNFBL achieved (DNNFBL+PSO)

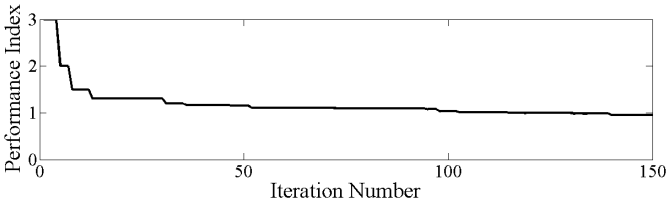

Fig. 6. Performance index evolution with PSO optimization

achieved a performance index of 0.93, which is an improvement of 68% from the PID-based AVSS. This infers that the proposed DNNFBL+PSO control scheme outperformed the PID-controlled system. However, this does not provide any information regarding the degree to which the conflicting performance criteria have been resolved for these methods.

4. SIMULATION RESULTS AND DISCUSSION

System performance is examined for the case where a deterministic road disturbance excites the AVSS during simulations in the Matlab/Simulink environment. Numerical experimentation shows that the performance of the rear right suspension system was the worst, and hence its results will be presented here. The suspension travel and tyre dynamic load responses are shown in Figures 7 and 8. Performance criterion relating to vehicle ride comfort (body-heave acceleration) is presented in Figure 10.

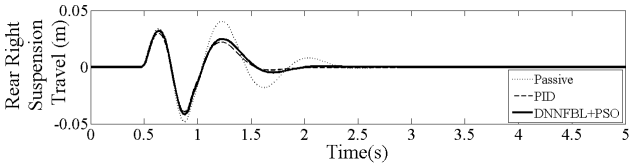

Fig. 7. Suspension travel response for PVSS and AVSS cases

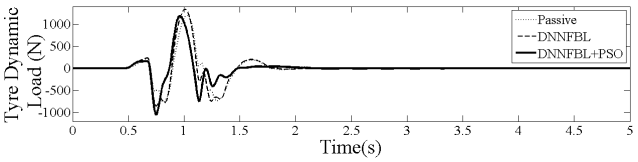

Fig. 8. Tyre dynamic load response for PVSS and AVSS cases

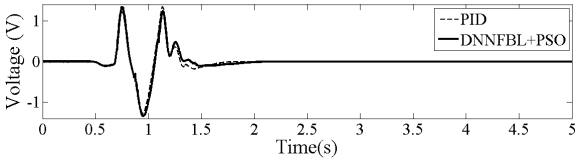

Fig. 9. Variation of control input supply the AVSS cases

Figure 7 shows that both AVSS controllers achieved superior settling times, better transient behaviour with minimal oscillations, and immediate damping once the disturbance had been passed. In road holding, both AVSS cases did not improve upon the PVSS in terms of peak values. On the other hand the DNNFBL+PSO case obtained superiority over the PVSS for all the tyres but it only showed a marginal improvement for the rear right system. In relation to the response in this aspect, both AVSS exhibited few oscillations, quicker damping, with the

DNNFBL+PSO showing smaller consecutive peaks.

The voltage supplied for the PID-based AVSS case had marginally lower peak value. It did settle smoother than the DNNFBL+PSO case. In the criterion of body-heave acceleration (ride comfort), the DNNFBL+PSO AVSS outperformed the PID case by a substantial degree in peak values.

Improved ride comfort and road holding attained for the DNNFBL+PSO controller would intuitively require a larger actuator force to cancel out the disturbance forces. However, the opposite occurred and this highlights that the PSO optimization and adaptive nature of the intelligent controller has a major impact on the system.

Analysis of the results shows that the DNNFBL+PSO had a better performance and found a better compromise between conflicting trade-offs than that of both the PID and PVSS cases. This concludes that soft computing technique is a useful tool in improving system performance and resolving conflicting design trade-offs.

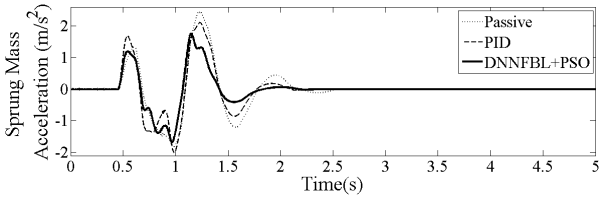

Fig. 10. Body-heave acceleration response for PVSS and AVSS cases

5. CONCLUSIONS

The main outcomes of this paper are:

- PSO proved to be effective in training DNN models.
- The advantages of PSO optimization were further realized as it assisted in improving the performance of the AVSS.
- DNNFBL+PSO attained the best performance index and successfully resolved the conflicting design requirements.

REFERENCES

Aldair, A.A. and Wang, W.J. (2010). Design of fractional order controller based on evolutionary algorithm for a full vehicle nonlinear active suspension system. *International Journal of Control and Automation*, 3(4), 33–46.

Alfi, A. and Fateh, M.M. (2011). Identification of nonlinear systems using modified particle swarm optimisation: A hydraulic suspension system. *Vehicle System Dynamics*, 49(6), 871–887.

Chiou, J.S., Tsai, S.H., and Liu, M.T. (2012). A PSO-based adaptive fuzzy PID-controllers. *Simulation Modelling Practice and Theory*, 26(8), 49–59.

Crews, J.H., Mattson, M.G., and Buckner, G.D. (2011). Multi-objective control optimization for semi-active vehicle suspensions. *Journal of Sound and Vibration*, 330(23), 5502–5516.

Dahunsi, O.A., Pedro, J.O., and Nyandoro, O.T. (2010). System identification and neural network based PID control of servo-hydraulic vehicle suspension systems. *Transactions of the South African Institute of Electrical Engineersion (SAIEE), Africa Research Journal (ARJ)*, 101(3), 93–105.

Eski, I. and Yildirim, S. (2009). Vibration control of vehicle active suspension system using a new robust neural network control system. *Simulation Modelling Practice and Theory*, 17(5), 778–793.

European Commission (2002). *Directive 2002/44/EC of the European Parliament and the Council of 25 June 2002 on the minimum health and safety requirements regarding the exposure of workers to the risk arising from physical agents (vibration)*. Official Journal of the European Communities, Luxembourg.

Garces, F.R., Becerra, V.M., Kambhampti, C., and Warwick, K. (2003). *Strategies for Feedback Linearisation: A Dynamic Neural Network Approach*. Springer, London.

Guclu, R. and Gulez, K. (2008). Neural network control of seat vibrations of a nonlinear full vehicle model using PMSM. *Mathematical and Computer Modelling*, 47(11-12), 1356–1371.

Kennedy, J. and Eberhart, R. (1999). The particle swarm: social adaptation in information-processing systems. In D. Corne, M. Dorigo, and F. Glover (eds.), *New Ideas in Optimization*, 379–387. McGraw-Hill, Cambridge, UK.

Lin, J., Lian, R.J., Huang, C.N., and Sie, W.T. (2009). Enhanced fuzzy sliding mode controller for active suspension systems. *Mechatronics*, 19(7), 1178–1190.

Norgaard, M., Ravn, O., Poulsen, N.K., and Hansen, L.K. (2000). *Neural Networks for Modelling and Control of Dynamic Systems: A Practitioner's Handbook*. Springer, Boston, MA.

Noura, H., Theilliol, D., Ponsart, J.C., and Chamseddine, A. (2009). *Fault-Tolerant Control Systems: Design and Practical Applications, Advances in Industrial Control*. Springer, London.

Pedro, J., Dangor, M., Dahunsi, O.A., and Ali, M.M. (2013). Differential evolution-based PID control of nonlinear full-car electrohydraulic suspensions. *Mathematical Problems in Engineering*, 2013(Article id. 261582), 1–13. URL `http://www.hindawi.com/journals/mpe/2013/`.

Pedro, J.O. and Dahunsi, O.A. (2011). Neural network based feedback linearization control of a servo-hydraulic vehicle suspension system. *International Journal of Applied Mathematics and Computer Science, AMCS*, 21(1), 137–147.

Pekgokgoz, R., Gurel, M., Bilgehan, M., and Kisa, M. (2010). Active suspension of cars using fuzzy logic controller optimized by genetic algorithm. *International Journal of Engineering and Applied Sciences*, 2(4), 27–37.

Wai, R.J., Lee, J.D., and Chuang, K.L. (2011). Real-Time PID control strategy for Maglev transportation system via particle swarm optimization. *IEEE Transactions on Industrial Electronics*, 58(2), 629–646.

Yagiz, N., Sakman, L.E., and Guclu, R. (2008). Different control applications on a vehicle using fuzzy logic control. *Sadhana*, 33(1), 15–25.